Medical Engineering and Physics 63 (2019) 26–32

Contents lists available at ScienceDirect

Medical Engineering and Physics

journal homepage: www.elsevier.com/locate/medengphy

Stress distribution in vertebral bone and pedicle screw and screw–bone load transfers among various fixation methods for lumbar spine surgical alignment: A finite element study

Ming Xu[a], James Yang[a,*], Isador Lieberman[b], Ram Haddas[b]

[a] Human-Centric Design Research Laboratory, Mechanical Engineering, Texas Tech University, Lubbock, TX, USA
[b] Texas Back Institute, Plano, TX, USA

ARTICLE INFO

Article history:
Received 2 February 2018
Revised 14 August 2018
Accepted 8 October 2018

Keywords:
Finite element method
Spine fusion surgery
Lumbar spine
Stress distribution
Screw–bone interaction force

ABSTRACT

This paper examines the stress distribution in the posterior fusion fixation, spinal range of motion (ROM), and the screw–bone interaction force obtained from various fixation methods of short-segment spine surgical alignment (SA) under five loading conditions (axial compression, flexion, extension, lateral bending, and axial rotation) provided by a FE spine model. The implant-instrumented FE spine model was validated against the experimental data in the literature. Among different fixation methods, fusing more spinal segments might help distribute the spinal load on the pedicle-screw to reduce the stress, screw force, and instability of the spine (range of motion). With longer rods, the additional intermediate screws are suggested to provide additional anchoring effect to the fixation device. However, the fact that inserting more screws also increases the stress concentration points on the rods should also be considered. Further this study supports the clinical observation that interbody cage can provide anterior support to the spine and reduce the loads on the posterior fixation devices. In both single-level and two-level fusion, IB reduced ROM, rod stress, and screw/bone interaction force.

1. Introduction

Pedicle-screw (PS)-based spine fusion is a standard treatment for degenerative spinal disorders which aims to consolidate the spine and restores the spinal stability [1,2]. Despite the continuous advances in PS designs and fixation techniques over the last two decades, failures of spinal implants, such as PS breakage [3], loosening and pullout, have not been fully eliminated in post-surgical spines [4–6]. Excessive stress concentrations within the vertebral bone after the PS-fixation of the spine is one major cause for the PS loosening or pullout while the excessive stress in the implants could result in the structural failure of the implants [7]. Risk of over fusion could also result in complications such as promimal junctional kyphosis (PJK) [21]. Revision surgeries are usually required after the failures of the implants, which carries with it significant risk for the patient and high cost for society [8]. It is of great clinical value to compare the stress distributions in the vertebral bones and spinal implants and screw–bone interaction forces associated with different fixation techniques in the fusion surgery [[2],[7],[9]]. By identifying and predicting the stress distributions, the possibility of spinal implant and bone failure could be analyzed. Additionally, analyzing the interaction force at the screw–bone interface could also provide insight regarding the force distributions between the spinal implants and spine.

In the literature, both cadaveric experimental and finite element (FE) studies have been conducted to predict the stress distributions in the spinal implants and spinal bony tissues after PS-instrumented surgery [2,7,9–11]. Compared with the cadaveric experimental studies, FE analysis has the advantages of lower cost, higher efficiency, and better capability of predicting the internal stress within the bone and applied to the spinal implants [12,13]. Ambati et al. [2] conducted FE analysis to compare the stresses in the posterior instrumentation from different fixation techniques of fusion surgery. Villa et al. ([29]) performed FE simulations and experimental validations to calculate the stress in the pedicle rod construct used in the SA under different loading conditions. Gornet et al. [11] also conducted FE simulations and experimental studies to compare the differences of stress in the traditional titanium rods in the rigid spinal fixation system and the poly-ether-ether-ketone (PEEK) rods in the semi-rigid fixation system. Although stress/strain information of the external cortical bone [7] and rods [10] could be measured experimentally, it remains challenging to use experimental approach to measure the interaction force and stress distribution internal to the bone and the PS bone interface.

* Corresponding author.
E-mail address: james.yang@ttu.edu (J. Yang).

https://doi.org/10.1016/j.medengphy.2018.10.003
1350-4533/

Table 1
Summary of material properties of spinal tissues.

Material	Modulus (Mpa)	Density (g/cm^3)	Poisson's ratio	Element type	References
Cortical bone	12,000	1.91	0.30	8-node solid element	[14]
Cancellous bone	100	1.87	0.20	8-node solid element	[14]
Posterior bony elements	3500	1.87	0.25	8-node solid element	[15]
Cartilaginous endplate	23.80	1.0003	0.40	8-node solid element	[15]
Annular ground substance	Hyperelastic (Mooney–Rivlin) c1 = 0.56, c2 = 0.14	1.0003	0.45	8-node solid element	[28]
Annular collagen fibers	Nonlinear stress–strain curve	1.0003		4-node shell element with rebar reinforced	[16]
Nucleus pulposus	Hyperelastic (Mooney–Rivlin) c1 = 0.12, c2 = 0.09	1.0003	0.4999	8-node solid element	[17]
Ligaments	Nonlinear stress–strain curves	1.0003		4-node shell element	[18]

FE studies are a feasible and necessary alternative to predict the internal stress to the bone and the stress applied to the PS. In previous studies, the effects of various parameters such as pedicle screw numbers, fusion level numbers, and interbody cage on the implant stress and spine biomechanical behavior (range of motion-ROM) have not been thoroughly studied for short-segment level fusions under physiological spinal loads. Although the patient-specific surgical plan is highly dictated by the spinal condition and anatomy, it is interesting to quantify how individual variables (screw numbers, fusion levels, and interbody cage) in different surgical plans will affect the implant stress, load transfer between the implant and spine and spinal ROM.

Thus, the objective of this study was to compare the stress value, stress distribution in the rods, the global ROM in the spine, and the screw/bone interaction force (resultant contact force between screw and bone) in different fixation methods of short-segment spine fusion [2,9,10] under five types of loading conditions (axial load of 500 N, 10 Nm in flexion, extension, lateral bending, and axial rotation), independently, while using a validated FE spine model. The six different fixation methods (Fig. 2) compared in this study include: (1) bilateral one-segment fixation with four pedicle screws (M1); (2) bilateral single-level fixation with four pedicle screws with an IB at L_3–L_4 level (M2) ; (3) bilateral two-segment fixations with four pedicle screws (M3); (4) intermediate unilateral fixation with five pedicle screws (M4); (5) bilateral intermediate fixation with six pedicle screws (M5); and (6) bilateral intermediate fixation with six pedicle screws with an IB at L_3–L_4 level (M6). These six methods were designed to study the effect of the screw numbers, fusion level numbers, and interbody cage on the spine and implant behaviors.

2. Methods

2.1. FE models

2.1.1. Lumbar spine FE model without implant

The segmental FE lumbar spine model (L2–L4) utilized in this study was obtained from one lumbar spine model of a 47-year old male healthy subject (Fig. 1) which was validated in our previous study [19]. Each vertebra consisted of a cancellous core surrounded by a cortical shell layer with thickness from 0.5 mm to 1 mm (Zander et al., [30]). At both ends of each vertebra, cartilaginous endplates were simulated with a thickness of 0.8 mm [13]. The facet cartilage joints were modeled as a soft frictionless contact with an initial gap of 0.5 mm (Zander et al., 2009). All seven major ligaments (anterior longitudinal ligament (ALL), posterior longitudinal ligament (PLL), flaval ligament (FL), facet capsular ligament (CL), intertransverse ligament (ITL), interspinous ligament (ISL), and supraspinous ligament (SSL)) were meshed by 4-node shell elements (Bowden et al., [24]). Local muscle forces and upper body weight

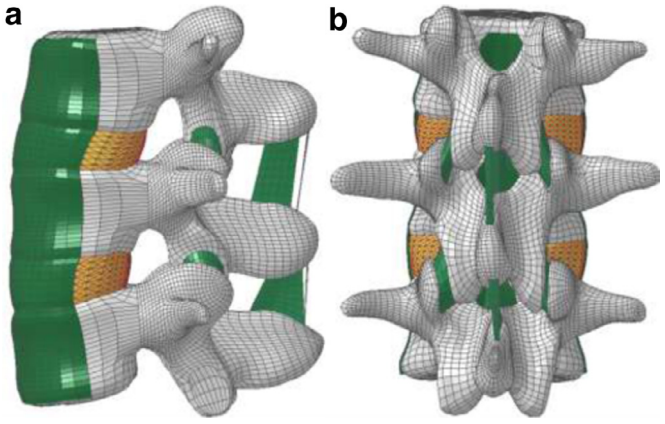

Fig. 1. FE model of a L_2–L_4 lumbar spine without implant: (a) side view; and (b) posterior view.

in lumbar spine were simulated by a compressive follower load with optimized path through the vertebrae (Dreischarf et al., [25]). Osseous tissues of the vertebrae and cartilaginous endplates in this study were modeled as isotropic homogeneous linearly-elastic materials [[14],[15]]. The intervertebral disc models were based on Schmidt et al. [27] with the following details: the annulus fibrosus was modeled into ground substance reinforced by collagen fibers. The nucleus pulposus and annular ground substance were modeled in an isotropic, hyper-elastic material using the Mooney–Rivlin material model (Schmidt et al., [28]). Eight layers of collagen fibers were generated radially in the annular ground substances using shell elements with rebar properties. The nonlinear mechanical behavior of the fibers was represented in a stress–strain curve [16]. Since the external layers of collagen fibers have greater stiffness than the internal layers, scalars were defined to weight the collagen fibers in different layers (outermost layers 1–2: 1.0, layers 3–4: 0.9, layers 5–6: 0.75, innermost layers 7–8: 0.65) to ensure the variations of stiffness. The orientations of the collagen fibers were defined with a 30- or 150-degree angle from the horizontal surface defined by the bottoms of intervertebral discs (Rohlmann et al., [26]). The mechanical behaviors of the ligaments were described using nonlinear stress–strain curves [18]. The material properties of different tissues are summarized in Table 1.

2.1.2. Spinal implants

One conical PS was tested in this study. The computer aided design (CAD) model of the PS was developed based on the dimensions and design variables reported by Chao et al. [3]: this PS had a length of 45 mm, inner diameter of 4.9 mm, and outer diameter of 6.5 mm. One PEEK interbody cage (IB) was implemented in this study with a posterior height of 9 mm, an anterior

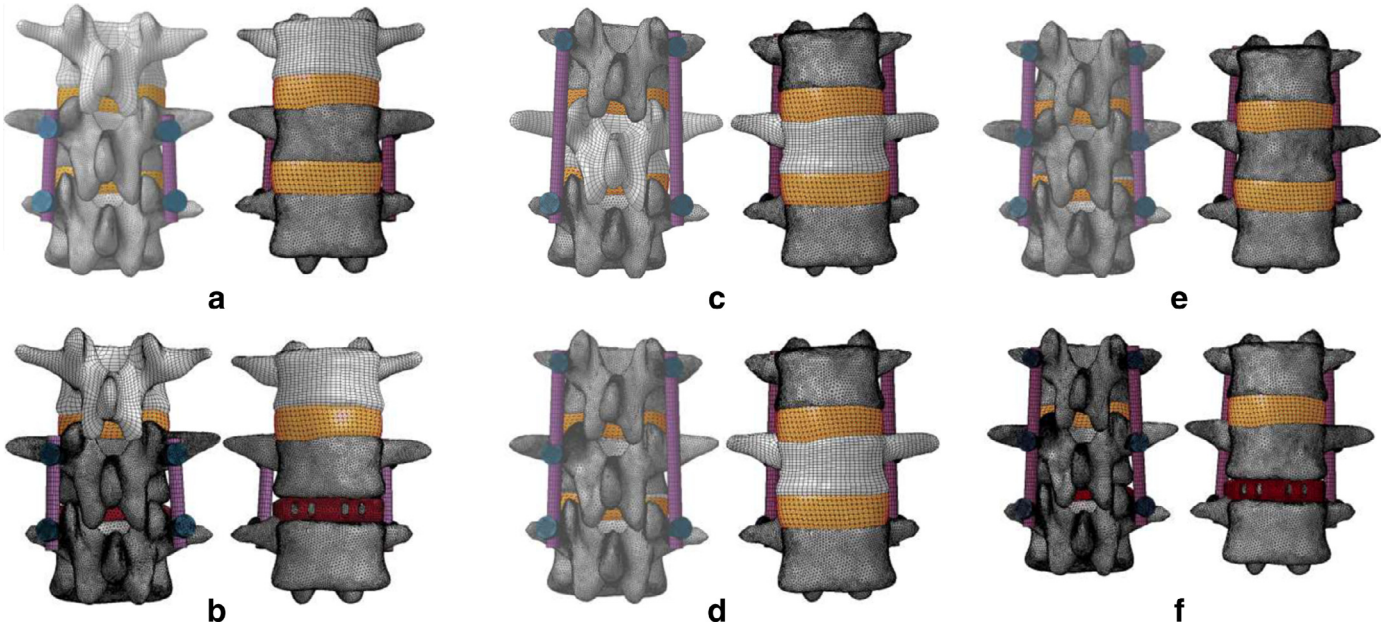

Fig. 2. Posterior and anterior views of instrumented lumbar spine FE model using different short-segment fixation methods: (a) method 1 (M1); (b) method 2 (M2); (c) method 3 (M3); (d) method 4 (M4); (e) method 5 (M5); and (f) method 6 (M6).

height of 12 mm, width of 15 mm, and a lordosis angle of 15°. The rods in this study had circular cross section with a diameter of 6.0 mm [10]. The PS and IB were meshed with tetrahedral elements and the rods were meshed with hexahedral elements. Mesh convergence test was conducted and the final element number was 54,413 for each PS. The PS and rods were simulated as homogeneous linear-elastic material with a Young's modulus of 110 GPa and a poison's ratio of 0.3 [3,10]. The PEEK IB was assigned with a Young's modulus of 3.6 GPa and a Poisson's ratio of 0.36 [2].

2.2. FE models of the instrumented lumbar spine with different fixation methods

As shown in Fig. 3, the previously-validated FE lumbar spine model was instrumented with PSs and rods using different fixation methods [9,10]: (1) bilateral one-segment fixation with four pedicle screws (M1) shown in Fig. 2(a); (2) bilateral single-level fixation with four pedicle screws with an IB at L_3–L_4 level (M2) shown in Fig. 2(b); (3) bilateral two-segment fixations with four pedicle screws (M3) shown in Fig. 2(c); (4) intermediate unilateral fixation with five pedicle screws (M4) shown in Fig. 2(d); (5) bilateral intermediate fixation with six pedicle screws (M5) shown in Fig. 2(e); and (6) bilateral intermediate fixation with six pedicle screws with an IB at L_3–L_4 level (M6) shown in Fig. 2(f). The positioning of the PS in the vertebrae followed the geometrical prescriptions of the American Society for Testing Materials (ASTM) F1717 standard, where the screw angles and the orientation of the rods were kept identical with the experimental setup in the literatures [10,20]. Perfect tied connections between the PS and the attached rods were assigned in this study where no relative movement was permitted between the screw head and the rod [9,10]. The screw–bone connection was also simulated as perfectly tied connection with consideration of the compaction effect of the PS to the bone to represent the long-term PS/bone bond with solid fusion [3,22].

2.3. Loading conditions and boundary conditions

The inferior endplate of L_4 vertebra in all tested FE models was fully constrained in all degrees of freedom. The loading conditions were applied on the superior endplate of L_2. For each instrumented FE spine model, five loading conditions [10] were tested: (1) an axial load of 500 N; (2) a moment of 10 Nm in flexion direction; (3) a moment of 10 Nm in extension direction; (4) a moment of 10 Nm in left lateral bending; and (5) a moment of 10 Nm in left axial rotation.

Table 2
Percentage variation of the rod von Mises stress in six fixation methods.

	M1	M2	M3	M4	M5	M6
Axial compression	160.3 MPa	−38%	−14%	−26%	−26%	−42%
Flexion	95.4 MPa	−36%	−8%	−21%	−28%	−48%
Extension	70.8 MPa	−40%	−46%	−18%	−36%	−46%
Lateral bending	93.2 MPa	−38%	−11%	−7%	−17%	−36%
Axial rotation	117 MPa	−39%	−17%	−20%	−24%	−46%

2.4. Validation of PS-instrumented FE spine models

The FE models of the intact lumbar spine and the spinal implants were validated separately in our previous studies [19,23]. The FE models of PS-instrumented spine were validated against the experimental and simulation results reported by Villa et al. [10] using the von Mises stress of the pedicle rods predicted in the M5 models. ANOVA method was utilized to correlate the von Mises stress values of this study and those in the literature [10].

3. Results

3.1. FE model validation and von Mises stress in the rod

As shown in Fig. 3, the maximum von Mises stress values of the rods predicted in this study were consistent with the experimental results and FE simulation results reported by Villa et al. [10] ($R^2 = 0.9247$), which validated the FE models in this study.

The variation of the maximum rod von Mises stress in each fixation method was calculated and compared to that in M1 (Table 2). To illustrate the stress distribution in the rod, the von Mises stress contour plots of the rod were generated for all the six fixation methods in flexion in consistent color scale (0–96 MPa) (Fig. 4).

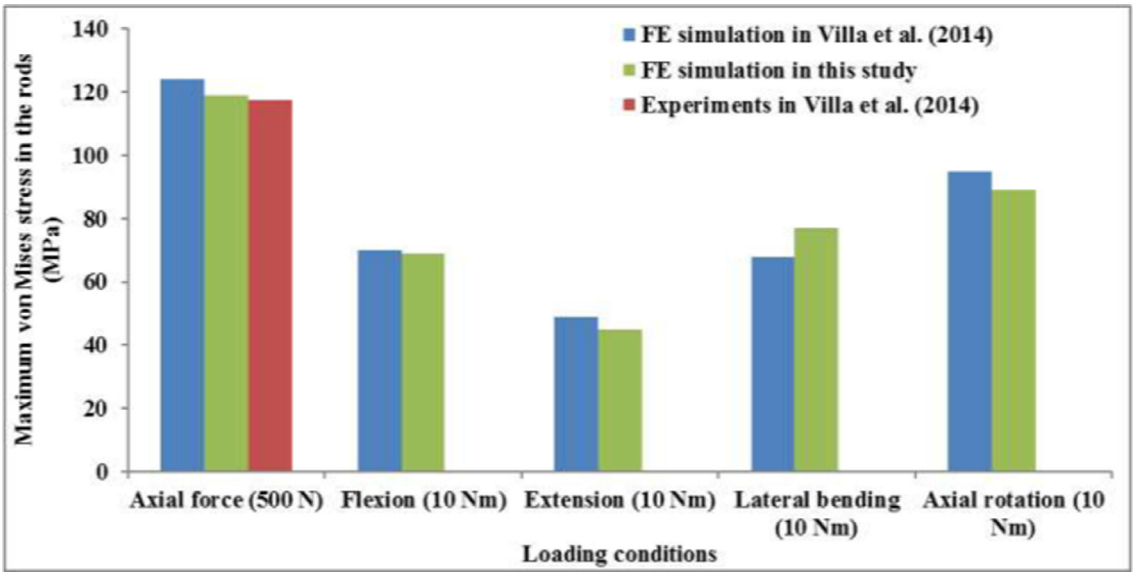

Fig. 3. Implant-instrumented spine FE model validations: comparison of maximum von Mises stress of the rods predicted in this study (M5) and that reported in the literature [10].

As shown in Table 2, the axial compression force of 500 N produced the largest von Mises stress in the rod among all five test loading conditions in M1 (160.3 MPa). Within the four pure bending loading conditions (flexion, extension, lateral bending, and axial rotation), axial rotation produced the largest von Mises stress (117 MPa) in the rod for all the six fixation methods, whereas flexion/extension produced the smallest (flexion/extension: 95.4 MPa/70.8 MPa). With IB, M2 reduced up to 40% of rod stress compared to M1, which generally reduced more rod stress than the configurations without interbody. With one more level fused, M6 reduced more rod stress than M2 did. With one more level fixed than M1 with same number of screws, M3 reduced considerably more rod stress in all loading conditions compared to M1 (between −8% and 46%). From M3 to M5, same level of fixation was conducted with increasing number of screws. As more screw inserted, more rod stress was reduced in all loading conditions except for extension in M3 (axial compression: −14% to −26%, flexion:−8% to −28%, extension: −46% to −36%, lateral bending: −11% to −17%, axial rotation: −17% to −24%). With IB inserted at L_3–L_4, M6 reduced considerably more rod stress than M5 did in all loading conditions (between −36% and −48%).

As shown in Fig. 4, the maximum von Mises stress occurred on the rod adjacent to the screw/rod connecting area in all the six fixation methods. In M1 and M2, the maximum rod von Mises stress concentrated at the rod/screw connecting area. Comparing M1 and M3: with shorter rod (M1), higher level of stress concentration occurred on the rod whereas stress tended to distribute on larger area on rod with extended rod (M3). In M4, three screws were attached on the left rod while two screws were attached to the right rod. The stress concentrated notably more on the left rod adjacent to the intermediate screw while the stress on the right rod tend to be more distributed. In M5 and M6, the maximum von Mises stress concentrated on the intermediate screw in both rods.

3.2. Range of motion

The variation of the global ROM of spine model with each fixation method was calculated and compared to that in M1 (Table 3).

As shown in Table 3, the flexion produced the largest ROM in the rod among four bending loading conditions in M1 (7.1°) followed by lateral bending (6.4°) whereas extension produced the smallest (3.8°). With IB inserted, M2 reduced up to 20% of global ROM in M1, which is greatly lower than those with two-level fusion (M2–M6). With one more level fixed using the same number of screws, M3 reduced considerably more ROM in all loading conditions compared to M1 (between −27% and −53%). With same fusion level, increasing the number of screws did not significantly affect the global ROM of the spine models (flexion: from −41% to −49%, extension: from −53% to −59%, lateral bending: from −52% to −59%, axial rotation: from −27% to −35%). With an IB inserted at L_3–L_4, M6 reduced significantly more ROM than M5 did in all loading conditions.

Table 3
Percentage variation of the global range of motion of spine model with six fixation methods.

	M1	M2	M3	M4	M5	M6
Flexion	7.1°	−15%	−41%	−45%	−49%	−62%
Extension	3.8°	−18%	−53%	−55%	−59%	−89%
Lateral bending	6.4°	−20%	−52%	−56%	−59%	−74%
Axial rotation	5.2°	−12%	−27%	−31%	−35%	−55%

Table 4
Percentage variation of the maximum screw/bone interaction force in six fixation methods.

	M1	M2	M3	M4	M5	M6
Axial compression	89 N	−53%	−21%	−6%	−35%	−69%
Flexion	108 N	−65%	1%	−9%	−76%	−86%
Extension	103 N	−54%	2%	−5%	−73%	−83%
Lateral bending	78 N	−43%	14%	−28%	−47%	−68%
Axial rotation	171 N	−44%	−11%	−4%	−44%	−56%

3.3. Maximum interaction force between the PS and vertebra

The variation of the maximum screw/bone interaction force in each fixation method was calculated and compared to that in M1 (Table 4).

As shown in Table 4, the axial rotation produced the largest screw force in the rod among all five test loading conditions in M1 (171 N). With IB inserted at L_3–L_4, M2 reduced up to 65% screw forces than M1 did. Comparing M2 with M6, M6 reduced up to 29% more screw force than M2 did with one more level of

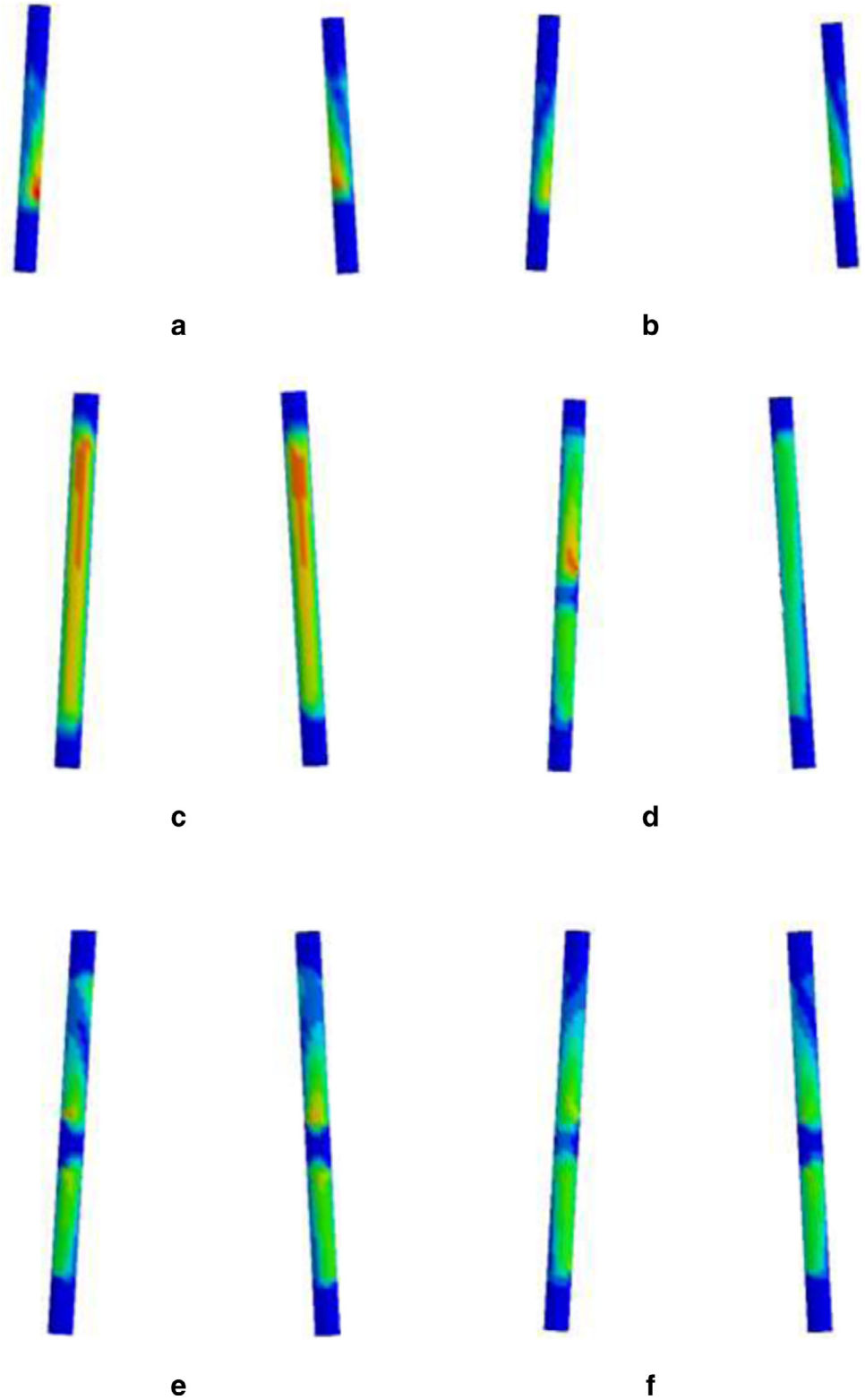

Fig. 4. Stress contour plots of the rods in six fixation methods: (a) M1; (b) M2; (c) M3; (d) M4; (e) M5; and (f) M6 (color scale 0–96 MPa).

fusion and two more screws to share the force. With one more level fixed using the same number of screws, M3 considerably reduced the screw force in axial compression (−21%) and axial rotation (−11%) whereas achieved comparable screw force in flexion/extension (1%/2%) and increased that in lateral bending (14%). With same level of fixation with increasing number of screws from M3 to M5, more screw force was reduced in all loading conditions (axial compression: −21% to −35%, flexion: 1% to −76%, extension: 2% to −73%, lateral bending: 14% to −47%, axial rotation: −11% to −44%). With IB inserted at L_3–L_4, M6 reduced considerably more screw force than M5 did in all loading conditions (axial compression: from −35% to −69%, flexion: from −76% to −86%, extension:

from −73% to −83%, lateral bending: from −47% to −68%, axial rotation: −44% to −56%).

Discussion

The present study primarily focused on comparing the effects of different fixation methods on the implant stress and load transfer between the implants and spine, which is intended to reveal the relative variations in the spinal biomechanics when changing the screw/rod configurations. It will be better to understand how individual parameters such as screw numbers, fusion levels, and interbody cage in different surgical plans will affect the spinal ROM, implant stress, and load transfer between the implant and spine. Six posterior short-segment fusion techniques were tested and compared, which were widely used to treat thoracolumbar burst fractures, scoliosis, and spondylolisthesis [2,9,10]. The implant-instrumented spine FE models were validated against the experiments reported by Villa et al. [10], where the von Mises stress in the pedicle rod predicted in this study was consistent with the experimental data. The variations of implants investigated in this study included a number of fused levels, number of pedicle screws inserted, and with or without an IB.

The von Mises stress in the rod could provide insights of the rod fracture risk. In general, the present study showed that more fixed spinal levels, more screws, and inserting the IB would reduce the stress in the rods. However, it has been observed that stress concentration occurred adjacent to the screw/rod connecting points. With fewer screws attached, less stress concentration occurred on the rods, which might increase the rod survival rate in the long term. In both single-level and two-level fusions, inserting IB reduced the rod von Mises stress. The main reason was that the IB provided the anterior support to the fused vertebrae. FE study has advantages in predicting the stress/strain in the implants over the physical test using the strain gauge because the strain gauge can only provide stress/strain information on discrete points [10].

The screw/bone interaction force was investigated to show the load distribution between the vertebrae and the spinal implants. With the same fused level, increasing the number of screws could help reduce the screw force. This is because the load was distributed to more screws. It is also noticeable that M3, even with longer rods compared to M1, generated marginally a larger screw force in flexion/extension and considerable larger screw force in lateral bending than M1 did. Due to the absence of the intermediate screws, M3 failed to provide the intermediate anchoring points for the rods, which produced a longer cantilever distance in the rod and allowed a larger local spinal deformation at the intermediate level. The intermediate screws are able to provide an anterior force to the intermediate vertebra creating a lordosis effect to the spine, which was consistent with the findings reported by Li et al. [9]. If the intermediate screws exist, the rod stress tended to concentrate adjacent to the roots of the intermediate screws (Fig. 4), which suggested that the intermediate screws bear a considerable amount of load. In both single-level and two-level fusions, the IB provided anterior support to the spine and reduced the screw force, which is well consistent with clinical observations.

Measuring the ROM of the spine verifies the overall stiffness of the spine implant construct which provides a measure of the stability provided by the fixation. The present study showed that instrumenting more spine levels with longer rods reduced both the rod stress and the ROM of the spine model. With IB inserted, more ROM will be reduced at fused level, which indicates that IB could increase the stability in the spine fusion. IB greatly increased the stability at the inserted level in both single-level fusion and two-level fusion. However, previous study has suggested that overfusion might induce adjacent segment deterioration and PJK [2,21]. To possibly prevent such degeneration, some have suggested techniques such as tethering bands attached to the upper instrumented vertebra to facilitate a smoother biomechanical transition of the ROM [21]. The present study also found that increasing the screw density with the same fused levels does not affect the global ROM. This is due to the fact that the global stiffness of the spine is primarily determined by the rod and IB configurations and the screws only serve as connections between the rods and bones. However, as seen in Fig. 4(d), fewer screws will increase the local stress concentration effect on the rod.

Among the five loading conditions tested in this study, the axial compression load (500 N) produced the largest von Mises stress in the rod and the screw–bone interaction force, which was consistent with the results reported by Villa et al. [10]. Among the four bending loading modes (flexion/extension, lateral bending, and axial rotation), the axial rotation generally produced the largest von Mises stress in implants and screw–bone interaction force, which was consistent with the general trends predicted in the literatures [2,10]. The loading conditions applied in this study were different from the physiological loads that resulted in the maximum ROM in each loading direction [12]. Dreischarf et al. [12] suggested that the FE spine models could also be tested by the loading conditions that combining pure bending moment and compression, which could better represent the physiological spinal loads.

The limitations of the present study should be taken into account. Since only static loading conditions were applied in this study, it is not possible to investigate the implant performance under long-term cyclic loading conditions. Although the maximum stress value predicted in this study was significantly lower than the material yield stress, long-term cyclic loads on the implants might result in the fatigue failure of the implants. In the situations of high-cycle fatigue failures of the implant, the breakage of individual fixation device might abruptly change stress or load distributions predicted in the present study. The present study cannot predict the failure history of the implants either. Another limitation of this study is that the residual stress in the implants introduced by the intraoperative rod bending procedure was not considered in the present study. The simplified bonded screw/rod connection might amplify the stress concentration effect adjacent to the screw/rod connecting points. Finally, linear-elastic and homogeneous material properties were assigned to bony tissues and the implants. Since the focus of this study is not predicting the post-yield behavior of the bony tissues and implants, it is acceptable to use linear-elastic material models to simulate the pre-yield elastic behaviors. However, linear-elastic material properties should be only utilized when the bony tissues and implants are under small deformations. To predict the failure and the yielding process of the bony tissues and implants under high-strain energy scenarios, nonlinear-elastic material properties are suggested.

Future studies will consider alternative stress in the implants in order to predict the high-cycle fatigue behavior of the implants. Since only short-segment spine model (L2–L4) were employed in this study, this study did not address the effects of global parameters (such as pelvic incidence and lordosis in the spine) on the biomechanical performance of the implants.

Conclusions

In summary, this study was able to compare the rod stress, the ROM of the spine and screw/bone interaction force in six different short-segment spine fixation methods under different loading conditions using the FE method. Among different fixation methods, instrumenting more spinal segments (increasing implant density) might help distribute the spinal load on the PS to reduce the stress, screw force, and instability of the spine (ROM). With longer rods, the additional intermediate screws are suggested to provide additional anchoring effect to the fixation device. However, the fact

that inserting more screws also increased the stress concentration points on the rods should also be considered. This study also supported the clinical observation that an interbody cage can provide anterior support to the spine and reduce the loads on the posterior fixation devices.

Conflict of interest

No.

References

[1] Brasiliense LBC, Lazaro BCR, Reyes PM, Newcomb A, Turner JL, Crandall DG, Crawford NR. Characteristics of immediate and fatigue strength of a dual-threaded pedicle screw in cadaveric spines. Spine J 2013;13:947–56.

[2] Ambati DV, Wright EK, Lehman RA, Kang DG, Wagner SC, Dmitriev AE. Bilateral pedicle screw fixation provides superior biomechanical stability in transforaminal lumbar interbody fusion: a finite element study. Spine J 2015;15:1812–22.

[3] Chao C-K, Hsu C-C, Wang J-L, Lin J. Increasing bending strength and pull-out strength in conical pedicle screws: biomechanical tests and finite element analyses. J Spinal Disord Tech 2008;21:130–8.

[4] Griza S, de Andrade CEC, Batista WW, Tentardini EK, Strohaecker TR. Case study of Ti6Al4V pedicle screw failures due to geometric and microstructural aspects. Eng Fail Anal 2012;25:133–43.

[5] Amaritsakul Y, Chao CK, Lin J. Biomechanical evaluation of bending strength of spinal pedicle screws, including cylindrical, conical, dual core and double dual core designs using numerical simulations and mechanical tests. Med Eng Phys 2014;36:1218–23.

[6] Elder BD, Holmes SL, Goodwin C, Kosztowski TA, Lina IA, Locke JE, Witham TF. The biomechanics of pedicle screw augmentation with cement. Spine J 2015;15:1432–45.

[7] Newcomb AGUS, Baek S, Kelly BP, Crawford NR. Effect of screw position on load transfer in lumbar pedicle screws: a non-idealized finite element analysis. Comput Methods Biomech Biomed Eng 2017;20:182–92.

[8] Martin BI, Franklin GM, Deyo RA, Wickize TM, Lurie JD, Mirza SK. How do coverage policies influence practice patterns, safety, and cost of initial lumbar fusion surgery? A population-based comparison of workers' compensation systems. Spine J 2014;14(7):1237–46.

[9] Li CQ, Zhou Y, Wang HW, Liu J, Xiang LB. Treatment of unstable thoracolumbar fractures through short segment pedicle screw fixation techniques using pedicle fixation at the level of the fracture: a finite element analysis. Plos One 2014;9:e99156.

[10] Villa T, La Barbera L, Galbusera F. Comparative analysis of international standards for the fatigue testing of posterior spinal fixation systems. Spine J 2014;14:695–704.

[11] Gornet MF, Chan FW, Coleman JC, Murrell B, Nockels RP, Taylor BA, Lanman TH, Ochoa JA. Biomechanical assessment of a PEEK rod system for semi–rigid fixation of lumbar fusion constructs. J Biomech Eng – Trans ASME 2011;133(8). 081009-081009-12.

[12] Dreischarf M, Zander T, Shirazi-Adl A, Puttlitz CM, Adam CJ, Chen CS, Goel VK, Kiapour A, Kim YH, Labus KM, Little JP, Park WM, Wang YH, Wilke HJ, Rohlmann A, Schmidt H. Comparison of eight published static finite element models of the intact lumbar spine: predictive power of models improves when combined together. J Biomech 2014;47:1757–66.

[13] Ayturk UM, Puttlitz CM. Parametric convergence sensitivity and validation of a finite element model of the human lumbar spine. Comput Methods Biomech Biomed Eng 2011;14:695–705.

[14] Kiapour A, Ambati D, Robert W, Goel V. Effect of graded facetectomy on biomechanics of dynesys dynamic stabilization system. Spine 2012;37(10):581–9.

[15] Lu Y, Hutton W, Gharpuray V. Do bending, twisting, and diurnal fluid changes in the disc affect the propensity to prolapse? A viscoelastic finite element model. Spine 1996;21:2570–9.

[16] Shirazi-Adl A, Ahmed A, Shrivastava S. Mechanical response of a lumbar motion segment segment in axial torque alone and combined with compression. Spine 1986;11(9):914–27.

[17] Schmidt H, Galbusera F, Rohlmann A, Shirazi-Adl A. What have we learned from finite element model studies of lumbar intervertebral disc in the past four decades. J Biomech 2013;46:2342–55.

[18] Eberlein R, Holzapfel G, Frohlich M. Multi-segment FEA of the human lumbar spine including the heterogeneity of the annulus fibrosus. Comput Mech 2004;34:147–63.

[19] Xu M, Yang J, Lieberman IH, Haddas R. Lumbar spine finite element model for healthy subjects: development and validation. Comput Methods Biomech Biomed Eng 2017;20(1):1–20.

[20] Barbera LL, Galbusera F, Villa T, Costa F, Wilke H. ASTM F1717 standard for the preclinical evaluation of posterior spinal fixators: can we improve it. Proc Inst Mech Eng H: J Eng Med 2014;228(10):1014–26 October 15, 2014.

[21] Bess S, Harris J, Turner A, LaFage V, Smith J, Shaffrey C, Schwab F, Haid R. The effect of posterior polyester tethers on the biomechanics of proximal junctional kyphosis: a finite element analysis. J Neurosurg: Spine 2017;26(1):125–33.

[22] Chazistergos P, Ferentinos G, Magnissalis A, Kourkoulis SK. The pull-out strength of transpedicular screws in posterior spinal fusion. Proceedings of the sixteenth European conference of fracture. Greece: Alexandroupolis; 2006. p. 417–18.

[23] Xu M, Yang J, Lieberman IH, Haddas R. Finite element method-based study for effect of adult degenerative scoliosis on the spinal vibration characteristics. Comput Biol Med 2017;84(2017):53–8.

[24] Bowden AE, Guerin HL, Villarraga ML, Patwardhan AG, Ochoa JA. Quality of motion considerations in numerical analysis of motion restoring implants of the spine. Clinical Biomechanics 2008;23(5):536–44.

[25] Dreischarf M, Zander T, Bergmann G, Rohlmann A. A non-optimized follower load path may cause considerable intervertebral rotations. Journal of Biomechanics 2010;43:2625–8.

[26] Rohlmann A, Burra NK, Zander T, Bergmann G. Comparison of the effects of bilateral posterior dynamic and rigid fixation devices on the loads in the lumbar spine: a finite element analysis. European Spine Journal 2007;16(8):1223–31.

[27] Schmidt H, Galbusera F, Rohlmann A, Zander T, Wilke HJ. Effect of multilevel lumbar disc arthroplasty on spine kinematics and facet joint loads in flexion and extension: a finite element analysis. European Spine Journal 2012;21(Sppl 5):S663–74.

[28] Schmidt H, Heuer F, Simon U, et al. Application of a new calibration method for a three-dimensional finite element model of a human lumbar annulus fibrosus. Clinical Biomechanics 2006;21(4):337–44.

[29] Villa T, La Barbera L, Galbusera F. Comparative analysis of international standards for the fatigue testing of posterior spinal fixation systems. Spine Journal 2014;14(4):695–704.

[30] Zander T, Rohlmann A, Bergmann G. Influence of different articicial disc kinematics on spine biomechanics. Clinical Biomechanics 2009;2(4):135–42.